Open access • Journal Article • DOI:10.1109/48.262305

The estimation of the shape of an array using a hidden Markov model — Source link

Barry G. Quinn, R.F. Barrett, Peter J. Kootsookos, S.J. Searle

Institutions: Salisbury University, Cooperative Research Centre

Published on: 01 Oct 1993 - IEEE Journal of Oceanic Engineering (IEEE)

Topics: Markov model, Hidden Markov model, Covariance matrix and Estimation theory

THE ESTIMATION OF THE SHAPE OF AN ARRAY USING A HIDDEN MARKOV MODEL

Thursday 25th February, 1993

Barry G. Quinn[1], Ross F. Barrett[1],
Peter J. Kootsookos[2] and Stephen J. Searle[2]

I INTRODUCTION

Degradation of performance occurs when beamforming is carried out on the sensor outputs of an acoustic towed array which is not straight. However, much of this performance loss can be recovered if the positions of the sensors can be estimated.

Two different approaches can be applied to array shape estimation. In the first, the array is fitted with heading and depth sensors along its length, and a physical model for the propagation of shape perturbations along the array is applied. This technique assumes that most of the array deformation is a result of tow-point induced motion. The array motion is governed by a partial differential equation known as the Paidoussis equation [1]. Examples of the application of this method are given by Kennedy [2], Dowling [3], Gray et al [4] and Riley et al [5].

[1]Maritime Operations Division, Defence Science and Technology Organisation, P.O. Box 1750, Salisbury 5108, AUSTRALIA

[2]Cooperative Research Centre for Robust and Adaptive Systems, DSTO site, P.O. Box 1750, Salisbury 5108, AUSTRALIA

An alternative approach to array shape estimation requires the presence of an acoustic source in the far field. Data from the hydrophones themselves are used to estimate the sensor positions. Ferguson [6] and Ferguson et al [7] describe two techniques that use this approach. The first is an optimisation technique, where the "sharpness" is calculated by integrating the product of the beam output power squared and the sine of the beam steer angle over all beam steer angles from forward endfire to aft endfire. The other method uses the eigenvector corresponding to the largest eigenvalue of the cross-spectral matrix to extract the phase of the signal at each of the hydrophones.

In this paper we present an alternative Hidden Markov model (HMM) method for array shape estimation using an acoustic far-field source. The distortion of the array from linearity is modelled by a hidden Markov chain. A measurement sequence is constructed from the Fourier coefficients of the various hydrophone outputs at the frequency of the far-field source. The likelihood of possible array shapes conditioned on the observed measurement sequence can be calculated using standard probability theory. The Viterbi algorithm enables a maximum likelihood estimate of the array shape to be obtained efficiently. The technique is formally very similar to the HMM estimation of frequencies from acoustic data described by Streit and Barrett [8] and Barrett and Holdsworth [9].

In Section II we discuss a model for the array and estimation techniques and in Section III the results of some simulations.

II THEORETICAL CONSIDERATIONS

II-A Array model

We make the assumption in this paper that the array consists of J sensors separated by straight segments of fixed length d. The incoming farfield signal is assumed to be sinusoidal, with additive spatially white noise not necessarily Gaussian or temporally white. The signal received at sensor $j \in \{0, 1, \ldots, J-1\}$ at time t seconds is thus

$$X_j(t) = \rho \cos\left\{\phi + 2\pi f\left[t - (x_j \sin\theta - y_j \cos\theta)/c\right]\right\} + \varepsilon_j(t)$$

where

(i) (x_j, y_j) is the position of the jth sensor, (x_0, y_0)=(0,0) and (x_1, y_1)=$(d, 0)$;

(ii) θ is the angle between the first array segment and the wavefront of the signal;

(iii) ρ and ϕ are the (constant) amplitude and initial phase of the sinusoid at sensor 0;

(iv) f is the frequency of the sinusoid and c is the speed of the signal;

(v) $\{\varepsilon_j(t); t \geq 0\}$ are uncorrelated (in j) stationary stochastic processes with common spectral density.

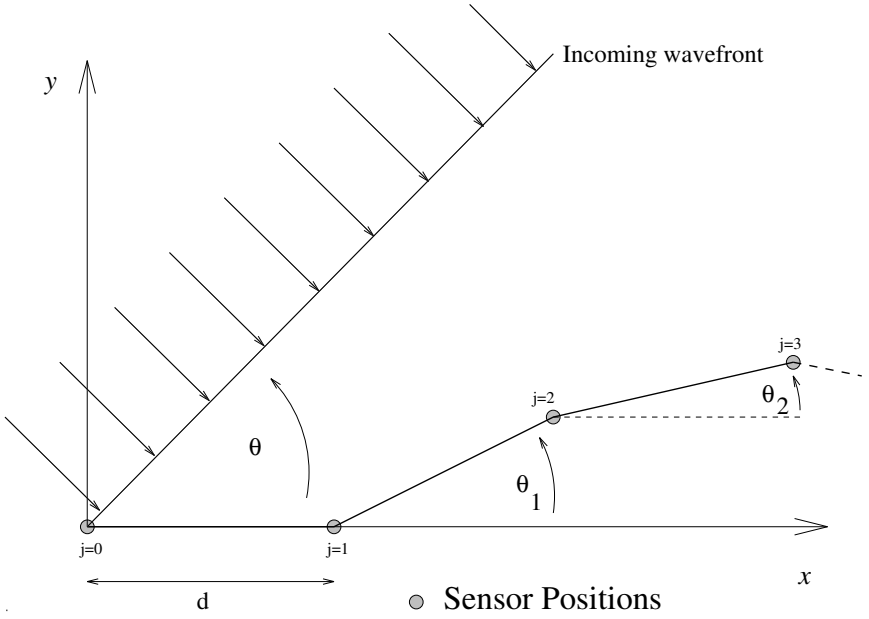

Figure 1: Wavefront arriving at array, and sensor positions

Conditions (i) and (ii) are imposed because the sensor positions as well as the bearing are unknown. The coordinate system is specified by having the first array segment coincident with the interval (0, 0)−(0,d), and θ may therefore be interpreted as the bearing of the source producing the signal from that first line segment. These definitions are essentially arbitrary, but are needed in order that both the shape and the bearing may be estimated in the absence of other directional measurements obtained, for example, by compasses. A more realistic definition of "bearing" would be the angle between the wavefront and some line of best fit through the array, and this is the approach we shall adopt in the post-processing stage. It should also be noted that although the model above incorporates only one sinusoid, the approach

that we take uses only the Fourier coefficients at one frequency, so that components at other frequencies will have negligible impact on the results.

Because the array segments are all straight and of the same length d, the coordinates of sensors 2 through $J-1$ may be parametrised in terms of $J-2$ angles: the angles between the last $J-2$ segments and the first. Thus, for $j = 1, \ldots, J-1$,

$$x_j + iy_j = d \sum_{k=0}^{j-1} \exp(i\theta_k) \tag{1}$$

where θ_0 is 0 by definition.

II-B Maximum likelihood array shape estimation

The HMM technique developed in Section II-C will utilise the Fourier coefficients at a frequency near f calculated from the signal received at times $0, 1/N, \ldots, (T-1)/N$. To this end, put

$$Y_j(\lambda) = \sum_{n=0}^{T-1} X_j(n/N) \exp(-i2\pi\lambda n/N)$$

calculated, say, by the fast Fourier transform and let $Y_j = Y_j(\tilde{f})$, where $\tilde{f}$ is some frequency of interest close to f ($\tilde{f}$ may correspond, for example, with a local maximum of the sum of the periodograms). Then

$$Y_j = U_j + \frac{T\tilde{\rho}}{2} \exp\left\{ i \left[\phi - \frac{2\pi f}{c} \left(x_j \sin\theta - y_j \cos\theta \right) \right] \right\}$$

$$= U_j + \frac{T\tilde{\rho}}{2} \exp\left\{ i \left[\phi - \frac{2\pi f d}{c} \left(\sum_{k=0}^{j-1} \sin(\theta - \theta_k) \right) \right] \right\}$$

plus smaller order terms, where $\sum_{k=0}^{-1}$ is zero by definition,

$$U_j = \sum_{n=0}^{T-1} \varepsilon_j(n/N) \exp(-i2\pi\tilde{f}n/N)$$

is the Fourier coefficient of the noise at $\tilde{f}$ and $\tilde{\rho}$ is close to ρ if $\tilde{f}$ is close to f. Since under very general conditions on $\{\varepsilon_j(t)\}$, amongst which is the condition that it have absolutely continuous spectral density which is nonzero at $\tilde{f}$, the U_j are, for T large, approximately complex Gaussian with zero means and independent real and imaginary parts having the same variance, say σ^2. An (approximate) maximum likelihood technique for estimating θ and $\theta_1, \ldots, \theta_{J-2}$ is obtained by forming the

likelihood of the Y_j as though the U_j were exactly complex Gaussian. It is easily seen that the maximum likelihood estimators are then obtained by minimising

$$\sum_{j=0}^{J-1} \left| Y_j - \frac{T\tilde{\rho}}{2} \exp\left\{ i \left[\phi - \frac{2\pi f d}{c} \left(\sum_{k=0}^{j-1} \sin(\theta - \theta_k) \right) \right] \right\} \right|^2$$

with respect to $\tilde{\rho}, \phi, \theta$ and $\theta_1, \ldots, \theta_{J-2}$. Thus θ and $\theta_1, \ldots, \theta_{J-2}$ are found by solving

$$\arg(Y_j / Y_{j-1}) = -\frac{2\pi f d}{c} \sin(\theta - \theta_{j-1}) \quad ; j = 1, 2, \ldots, J-1$$

II-C HMM array shape estimation

The approach of the estimation technique described in Section II-B assumes that the θ_j are fixed angles to be estimated. Under ideal circumstances, and certainly if the model were correct and the SNR high, the maximum likelihood estimator would be very accurate, notwithstanding the ambiguous solutions to the above equations. Under low SNR conditions, however, the variances of the real and imaginary components of the U_j may be so high compared with the square of $T\tilde{\rho}/2$ that the estimators have large variances. In such conditions, *prior information* is needed to decrease these variances. As the differences between the θ_j represent the angular deviations between consecutive segments of the array, one approach would be to maximise the likelihood function under the constraints that the $|\theta_j - \theta_{j-1}|$ were less than a certain tolerance suggested by such physical limitations in the array as flexibility. A simpler approach, and one that has gained much popularity recently, is to impose a statistical model on the θ_j, even though this model is not believed to be physically correct. In other words, the model is imposed only to obtain an estimation procedure. Such an approach has been used in Streit and Barrett [8] and Barrett and Holdsworth [9], where a technique for tracking frequency has been developed assuming that the true frequency in each time block is Markovian. As with all such hidden Markov models, the hidden states form a discrete set, so that the Viterbi algorithm may be used to find the state sequence which maximises the joint likelihood of the Y_j and the θ_j.

Let $\alpha_j = \theta_j - \theta_{j-1}$. We shall assume that $\alpha_1, \ldots, \alpha_{J-2}$ are independent and identically distributed with mean zero. For the purposes of the simulations of Section 3,

we shall also assume that they are discretised versions of normal random variables, but the technique described here requires only that the α_j be discrete independent random variables with known common probability function. There are several problems associated with a direct implementation of the hidden Markov method. One is that $\tilde{\rho}, \phi$ and the variances of the real and imaginary parts of the U_j must be known *a priori* . Another is that the argument of the complex exponential in (II-B) can exceed 2π in absolute value, resulting in considerable ambiguity. We shall thus work with the ratios of Fourier coefficients

$$R_j = \frac{Y_{j+1}}{Y_j} = \exp\left[-i\frac{2\pi fd}{c}\sin(\theta - \theta_j)\right]\frac{1+V_{j+1}}{1+V_j} \quad ; j = 0, 1, \ldots, J-2$$

where

$$V_j = \frac{2}{T\tilde{\rho}}\exp\left\{-i\left[\phi - \frac{2\pi fd}{c}\left(\sum_{k=0}^{j-1}\sin(\theta - \theta_k)\right)\right]\right\}U_j$$

The advantages in transforming in this way are that the number of parameters has been reduced by two: The distributions of the R_j depend only on the parameters of interest $\theta, \theta_1, \ldots, \theta_{J-2}$ and the common variance of the real and imaginary parts of the V_j, $\nu^2 = 2\sigma^2/(T\tilde{\rho}^2)$. The disadvantage is that the R_j are dependent random variables, whereas the Y_j were independent. The joint likelihood function of the R_j is thus not formed by multiplying the individual likelihoods. As the Viterbi algorithm only applies when the likelihood is multiplicative in this way, therefore, it would seem that it could not be used in this instance. There is nothing to prevent us, however, from forming the pseudo-likelihood which is constructed by multiplying the marginal likelihoods, and acting as though this were the correct likelihood. All that is expected is that there will be some loss of information owing to the nonuse of the dependence between the terms $\{1 + V_{j+1}\} / \{1 + V_j\}$ whose joint distribution does not depend at all on the parameters of interest.

Given the form of (II-C), it might be expected that using only the arguments (phases) of the R_j would result in further simplification of the problem. Unfortunately, this is not the case. The following result, the proof of which is contained in the Appendix, shows that the probability density functions of the R_j have extremely simple forms. Integrating out the moduli, however, can only be done numerically, resulting in prohibitive computational cost and inaccuracy.

Lemma 1 *Let $Z = \exp(i\xi)\frac{R+A}{R+B}$, where A and B are independent complex normal random variables whose real and imaginary parts are independent with zero means and common variances 1 and ξ and R are real constants. Then the pdf of Z is*

$$f_Z(z) = (2\pi)^{-1}(1+|z|^2)^{-2}\exp(-\frac{1}{2}R^2)\left(2+R^2+2\mathcal{S}\right)\exp\mathcal{S}$$

where

$$\mathcal{S} = \frac{R^2\Re\left[z\exp(-i\xi)\right]}{1+|z|^2}$$

The log of the pseudo-likelihood of $R_0, R_1, \ldots, R_{J-2}$ is thus, putting $R = \nu^{-1}$,

$$-(J-1)\log(2\pi\nu^2) - 2\sum_{j=0}^{J-2}\log\left(1+|R_j|^2\right)$$

$$+\sum_{j=0}^{J-2}\log\left\{2\nu^2+1+\frac{2\Re\left[R_j\exp(-i\xi_j)\right]}{1+|R_j|^2}\right\} - \frac{J-1}{2\nu^2} + \frac{1}{\nu^2}\sum_{j=0}^{J-1}\frac{\Re\left[R_j\exp(-i\xi_j)\right]}{1+|R_j|^2}$$

where

$$\xi_j = -\frac{2\pi fd}{c}\sin(\theta-\theta_j)$$

We shall use the notation of [8] in formulating the Viterbi algorithm. We shall identify the states of the HMM with the values taken on by the θ_j/q. The states of the HMM will thus be elements of $\{-K, 1-K, \ldots, 0, 1, \ldots, K\}$ where K is some integer. The log of the pdf of R_k at r, conditional on $\theta_k = jq$ is obtained from

$$\log b_j(r) = -\log(2\pi\nu^2) - 2\log\left(1+|r|^2\right) - (2\nu^2)^{-1}$$

$$+\log\left(2\nu^2+1+\frac{2\Re\left[r\exp\left\{i\frac{2\pi fd}{c}\sin(\theta-jq)\right\}\right]}{1+|r|^2}\right) + \frac{\Re\left[r\exp\left\{i\frac{2\pi fd}{c}\sin(\theta-jq)\right\}\right]}{\nu^2(1+|r|^2)}$$

The transition probabilities associated with the θ_j are simply calculated, as $\theta_j = \theta_{j-1} + \alpha_j$, where $\theta_0 = 0$ and the α_j are iid with zero mean. In this paper, we assume that the α_j are quantised versions of normal random variables with variances reflecting the likely distortion the array may undergo. Thus

$$a_{ij} = \Pr\{\theta_n = qj|\theta_{n-1} = qi\} = \Pr\{\alpha_n = q(j-i)\} = p_{j-i}$$

where

$$p_j = \Phi\left\{\frac{q(j+.5)}{\mu}\right\} - \Phi\left\{\frac{q(j-.5)}{\mu}\right\}$$

μ^2 is the variance of the underlying (continuous) deviations and Φ is the cumulative distribution function of the standard normal distribution. The initial state probabilities are easy to calculate in this instance, as θ_0 is 0 by definition. Thus $\pi_j = p_j$. We may now formulate the Viterbi algorithm for maximising the likelihood of the θ_j given the R_j (or, equivalently, the joint likelihood of the θ_j and the R_j), constructed as though the R_j were independent:

For fixed θ,

1. Let $\delta_1(k) = \log p_k + \log b_k(R_1)$; $k = -K, \ldots, 0, K$.

2. For $j = 2, \ldots, J-2$, let

$$\delta_j(k) = \log b_k(R_j) + \max_{-K \leq n \leq K} \{\delta_{j-1}(n) + \log p_{k-n}\}$$

and

$$\psi_j(k) = \arg \max_{-K \leq n \leq K} \{\delta_{j-1}(n) + \log p_{k-n}\}$$

3. The Viterbi score for θ is

$$\mathcal{V}(\theta) = \log b_0(R_0) + \max_{-K \leq n \leq K} \delta_{J-2}(n)$$

and the Viterbi track is calculated from $\hat{\theta}_j = qI_j$, where

$$I_{J-2} = \arg \max_{-K \leq n \leq K} \delta_{J-2}(n)$$

and

$$I_j = \psi_{j+1}(I_{j+1}) \ ; \ j = J-3, \ldots, 1$$

The estimator of θ is then $\hat{\theta} = \arg\max \mathcal{V}(\theta)$ and the estimators of the θ_j are those associated with the Viterbi track for $\hat{\theta}$. For reasons of symmetry, one need only consider $\theta \in (-\pi/2, \pi/2)$.

II-D Bearing estimation

There is an obvious difficulty associated with our parametrisation, namely, that the parameter θ is only the bearing of the signal from the first segment of the array. In the absence of any absolute directional information, the angle between the wavefront and a straight line of best fit through the array could more meaningfully

be considered as "bearing". Suppose that the above algorithm yields the positions $\{(x_j, y_j), j = 0, 1, \ldots, J-1\}$ for the sensors, using (1). Let $(\bar{x}, \bar{y})$ be the centroid of the estimated array. We wish to find γ such that, when the positions are rotated through γ and translated so that the centroid of the rotated array is the origin, to form $\left\{(x'_j, y'_j), j = 0, 1, \ldots, J-1\right\}, \sum_{j=0}^{J-1} \left(y'_j\right)^2$ is minimised. We thus minimise

$$\sum_{j=0}^{J-1} \left\{(x_j - \bar{x}) \sin\gamma + (y_j - \bar{y}) \cos\gamma\right\}^2 = A + B\cos(2\gamma) + C\sin(2\gamma)$$

where $A = \frac{1}{2}\sum\left\{(x_j - \bar{x})^2 + (y_j - \bar{y})^2\right\}, B = \frac{1}{2}\sum\left\{(y_j - \bar{y})^2 - (x_j - \bar{x})^2\right\}$ and $C = \sum(x_j - \bar{x})(y_j - \bar{y})$. We thus rotate the estimated array through $\hat{\gamma} = k\pi + \{\pi + \arg(B + iC)\}/2$, where k is an integer, and the estimate of bearing is $\hat{\theta} + \hat{\gamma}$.

II-E Data aggregation and the estimation of ν^2 and μ^2

The maximum likelihood and HMM techniques presented above may be also be used when circumstances require that data be aggregated. If Fourier coefficients are used to form sample spectral covariance matrices, then the dominant eigenvector of this matrix may be used in the same way as the vector of Y_j's was used above. If it can be assumed that the shape of the array does not change much over the aggregation time, the nett effect is to replace ν^2 by ν^2/K, where K is the number of time blocks used to form the spectral covariance matrix.

The problem remains of estimating the system parameters ν^2 and μ^2. Unfortunately, this is not as simple as maximising the "likelihood" given the R_j and the θ_j. What must be maximised is the "likelihood" given only the R_j, which is obtained by integrating the joint pdf of the R_j and the θ_j with respect to the values of the θ_j. This may be done directly, or by using the EM (Expectation-Maximisation) algorithm. Besides giving readily computable estimates of ν^2 and μ^2, the technique also provides estimates of the states which are continuous even though the states are discrete. These "conditional mean" estimates therefore often provide more realistic estimates of the states. The EM algorithm, however, converges slowly, and needs "good" initial estimates to guarantee convergence to the global maximiser of the likelihood. The details are outside the scope of this paper.

III SIMULATIONS

In this section we showcase the HMM bearing and array shape estimation procedure described in Section II-C by comparing it with the maximum likelihood method of Section II-B.

III-A Array Shape Generation

Two array shape models were used to generate the true array shapes used in these simulations: a deterministic sinusoidal model [6] and the stochastic model assumed in Section II-C. In Figure 2, plots of one realisation from the stochastic shape generation model and the (unchanging) sinusoidal shape are shown.

All shapes plotted in this section are rotated so that the array centroid lies at (0,0) and the least squares fit straight line through the sensor positions is horizontal.

The sensor to sensor angular variation (the α_j, $j = 1, \ldots, J-2$) of the HMM shape generation procedure is assumed to be the discretisation of a normally distributed random variable with standard deviation μ.

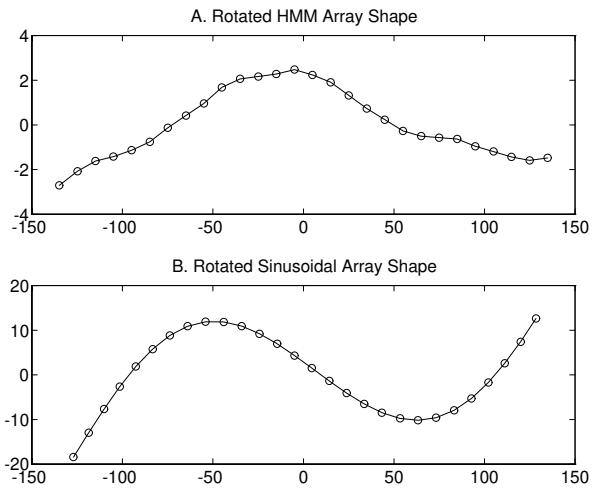

Figure 2: Examples of the shapes generated by the HMM and sinusoidal array shape generation procedures.

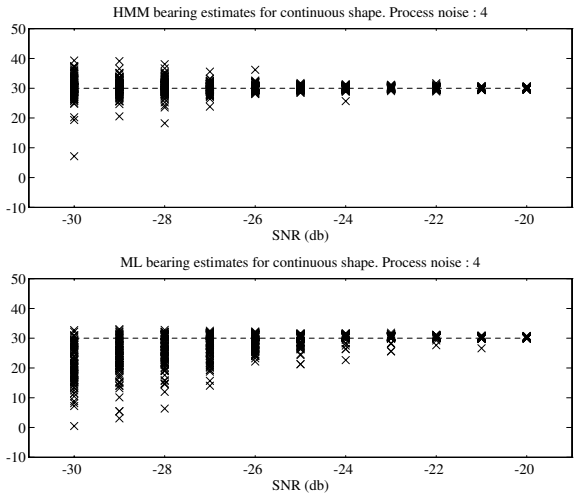

Figure 3: Scatter plot of bearing (degrees) versus SNR (dB) scatter plot for $\mu = 4$ degrees and HMM shape. The dashed line indicates the true bearing.

III-B Bearing Estimation Results — HMM Generated Shape

The following procedure was followed for $\mu = 4$ degrees and $\mu = 10$ degrees. This value was used both in the generation of the true shape and in the HMM shape estimation procedure. Also, the true value of ν (related to the SNR) was used. The SNR was varied from -20dB to -30dB with a decrement of 1dB. The SNR in dB is defined to be

$$10 \log_{10} \left(\frac{\rho^2}{2\sigma^2} \right)$$

where ρ and σ have been defined previously. For each SNR and μ a shape was generated using the hidden Markov model. For each of 100 replications, different initial phases were chosen (with $\phi \sim U(0, 2\pi)$) and different realisations of the complex noise process $\varepsilon_j(t)$ were generated. The shape, initial phases and noise processes were then used to generate the Fourier coefficients Y_j, $j = 0, \ldots, J-1$. Both the maximum likelihood and HMM bearing estimation procedures were applied to the data.

Figure 3 shows two scatter plots of the bearing estimates obtained by each method for the $\mu = 4$ case. The true bearing of 30 degrees ($\pi/6$ radian) is plotted as the dashed line. The root mean square errors versus SNR are plotted in Figure 4. Figures 5 and 6 show similar plots for the $\mu = 10$ case.

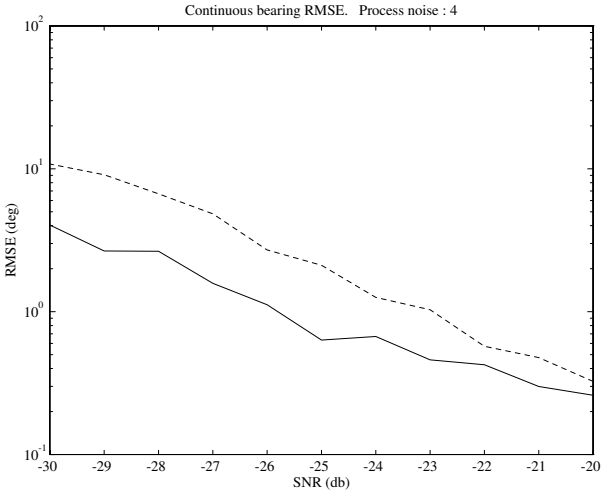

Figure 4: Root mean square error (in degrees) versus SNR (dB) for $\mu = 4$ degrees and HMM shape. The solid line shows the HMM technique results and the dashed line shows the maximum likelihood technique results.

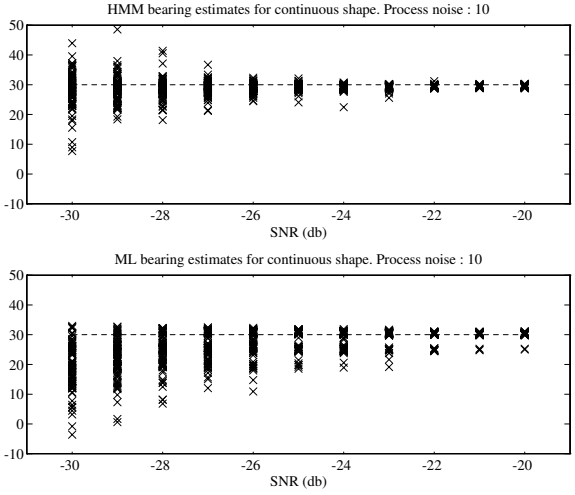

Figure 5: Scatter plot of bearing (degrees) versus SNR (dB) scatter plot for $\mu = 10$ degrees and HMM shape. The dashed line indicates the true bearing.

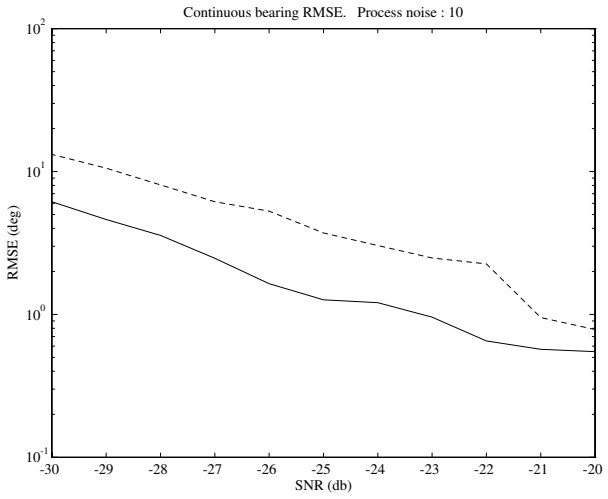

Figure 6: Root mean square error (in degrees) versus SNR (dB) for $\mu = 10$ degrees and HMM shape. The solid line shows the HMM technique results and the dashed line shows the maximum likelihood technique results.

III-C Bearing Estimation Results — Sinusoidal Shape

The previous results were to show the performance of the HMM technique when the data being processed is generated stochastically, with parameters precisely as assumed by the model. In order to demonstrate the robustness of the technique, we now use a sinusoidal true shape which is deterministically generated and so it is unclear how to choose the μ model parameter.

A similar procedure to the previous simulation was followed, except that the true shape used was the same for all SNR and μ combinations. The results of the simulations are depicted in Figures 7 to 10. Note that, for the $\mu = 4$ degrees case, there is a slight bias in the bearing estimation. This is reflected in Figure 8 where, for SNRs greater than -25dB, the maximum likelihood bearing estimator outperforms the HMM technique. For the HMM technique to work well, it would appear that μ should be selected greater than its true value. As a result, for this $\mu = 4$ degrees case, the array shapes estimated are smoother than the true shape. This extra smoothness may produce the observed biased bearing estimates. Another possible reason is that an HMM model with $\mu = 4$ may not be appropriate for a sinusoid with incremental angular standard deviation 4.

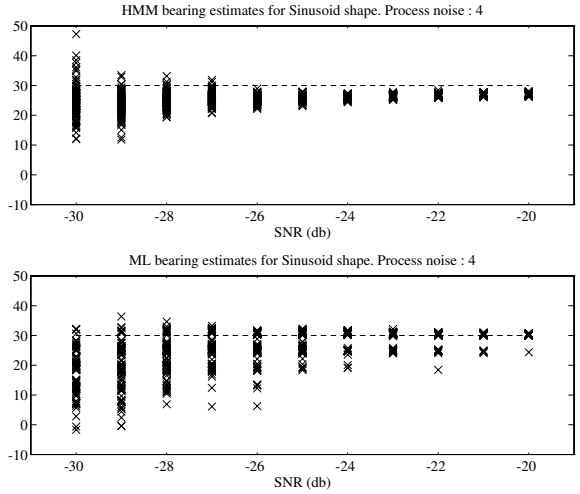

Figure 7: Scatter plot of bearing (degrees) versus SNR (dB) scatter plot for $\mu = 4$ degrees and sinusoidal shape. The dashed line indicates the true bearing.

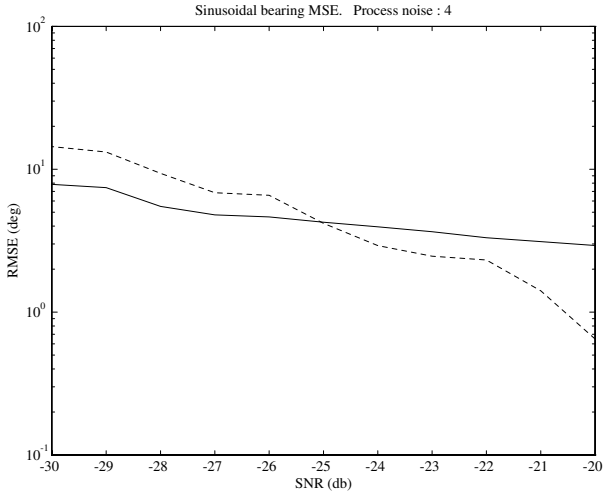

Figure 8: Root mean square error (in degrees) versus SNR for $\mu = 4$ degrees and sinusoidal shape. The solid line shows the HMM technique results and the dashed line shows the maximum likelihood technique results.

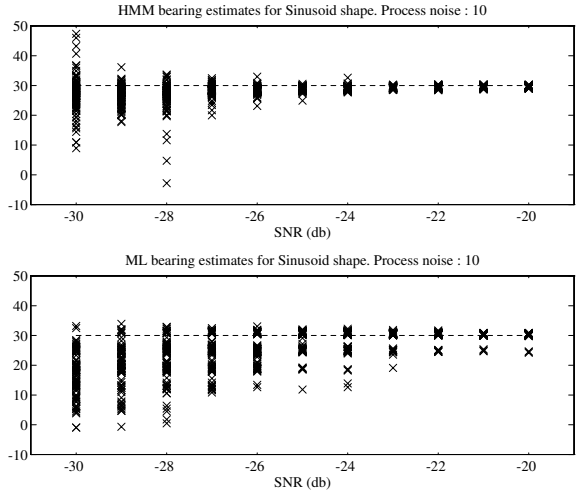

Figure 9: Scatter plot of bearing (degrees) versus SNR (dB) scatter plot for $\mu = 10$ degrees and sinusoidal shape. The dashed line indicates the true bearing.

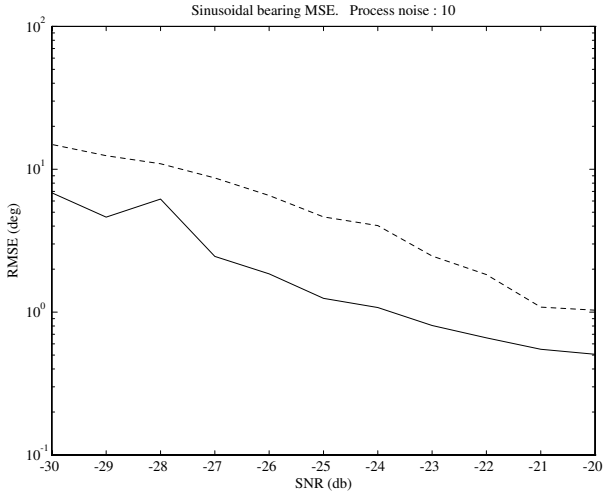

Figure 10: Root mean square error (in degrees) versus SNR (dB) for $\mu = 10$ degrees and sinusoidal shape. The solid line shows the HMM technique results and the dashed line shows the maximum likelihood technique results.

III-D Array Shape Estimation Examples

For this example, we generated 200 realisations of the Fourier coefficients Y_j at SNRs of -20dB and -30dB using a sinusoidal true shape.

Both the maximum likelihood and HMM array shape estimation procedures were carried out on each realisation, and the resulting estimated sensor positions plotted as the dots in Figures 11 and 12. Again all the shapes are rotated in accordance with Section II-D.

The true array shape is shown as the solid line.

The value of μ needed by the HMM array shape estimation algorithm is estimated as 4.26 degrees by simply finding the root mean square value of the α_j's for the given array shape.

The main points to note are:

- The value of μ given above is too low, as the -20dB example shows that the HMM-estimated shapes are smoother than the true shape. This may induce (as noted previously) a bias in the bearing estimates obtained via this technique.
- For low SNR (-30dB), the HMM shape estimates have a structure much more like a sinusoid than do the maximum likelihood estimates.

IV CONCLUSIONS

We have presented in this paper a hidden Markov technique for the estimation of the shape of an array. The technique uses the Fourier coefficients at a given frequency of a signal from a far-field acoustic source of opportunity. It may be also be used on the maximal eigenvector of a sample spectral covariance matrix. At low SNR the technique outperforms maximum likelihood techniques. There remain the problems of estimating the unknown system parameters. It is of course a simple matter to estimate the background SNR near the line of opportunity but the problem of estimating the shape deviation parameter μ is yet to be solved satisfactorily.

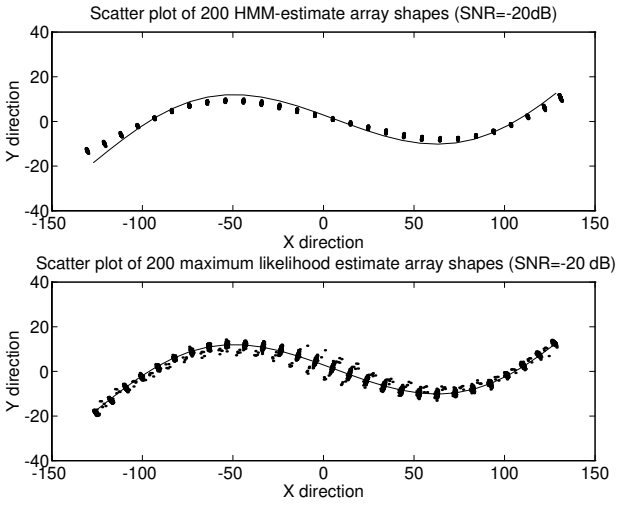

Figure 11: Sensor position scatter plots for the HMM (top) and maximum likelihood methods (bottom) for SNR = -20dB. The true array shape is indicated by the solid line.

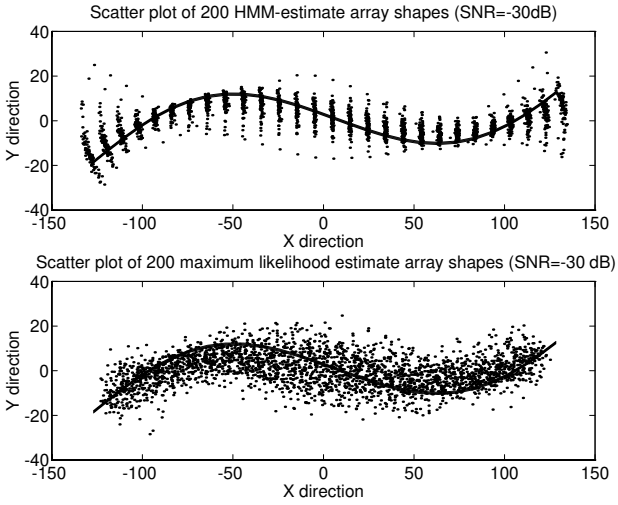

Figure 12: Sensor position scatter plots for the HMM (top) and maximum likelihood methods (bottom) for SNR = -30dB. The true array shape is indicated by the solid line.

ACKNOWLEDGEMENTS

The authors acknowledge the support of the Cooperative Research Centre for Robust and Adaptive Systems.

APPENDIX

PROOF OF LEMMA

Assume first that $\xi = 0$. Let $X = R + \Re A, Y = \Im A, U = R + \Re B, V = \Im B$. Then

$$Z = C + iD = \frac{XU + YV + i(YU - XV)}{U^2 + V^2}.$$

The transformation from X, Y, U, V to C, D, U, V is easily shown to have a Jacobian with determinant $(U^2 + V^2)^{-1}$. Consequently, the joint pdf of C, D, U and V is

$$f_{C,D,U,V}(c,d,u,v) = (2\pi)^{-2}(u^2+v^2)\exp\left\{-\frac{1}{2}\left[(u-R)^2 + v^2 + (uc - vd - R)^2 + (vc + ud)^2\right]\right\}$$

$$= \gamma(u^2+v^2)(2\pi)^{-2}(1+c^2+d^2)\exp\left(-\frac{1+c^2+d^2}{2}\left\{\left[u - \frac{R(c+1)}{1+c^2+d^2}\right]^2 + \left(v + \frac{Rd}{1+c^2+d^2}\right)^2\right\}\right)$$

where

$$\gamma = \exp\left\{-R^2 + \frac{R^2\left[(c+1)^2 + d^2\right]}{2(1+c^2+d^2)}\right\}(1+c^2+d^2)^{-1}$$

Thus

$$f_{C,D}(c,d) = \int_{-\infty}^{\infty}\int_{-\infty}^{\infty} f_{C,D,U,V}(c,d,u,v)\,du\,dv$$
$$= (2\pi)^{-1}\gamma\,\mathrm{E}\left(\mathcal{U}^2 + \mathcal{V}^2\right)$$

where $\mathcal{U}$ and $\mathcal{V}$ are independent normal random variables with the same variance $(1+c^2+d^2)^{-1}$ and means $\{R(c+1)\}/(1+c^2+d^2)$ and $(-Rd)/(1+c^2+d^2)$ respectively. Thus

$$f_{C,D}(c,d) = (2\pi)^{-1}\gamma\left\{\mathrm{var}\,\mathcal{U} + \mathrm{var}\,\mathcal{V} + [\mathrm{E}(\mathcal{U})]^2 + [\mathrm{E}(\mathcal{V})]^2\right\}$$

$$= (2\pi)^{-1}\gamma\left\{\frac{2}{1+c^2+d^2} + \frac{R^2\left[(c+1)^2+d^2\right]}{(1+c^2+d^2)^2}\right\}$$

$$= (2\pi)^{-1}\left(1+c^2+d^2\right)^{-2}\left(2 + R^2 + \frac{2cR^2}{1+c^2+d^2}\right)\exp\left(-\frac{1}{2}R^2 + \frac{cR^2}{1+c^2+d^2}\right)$$

$$= (2\pi)^{-1} \left(1 + |z|^2\right)^{-2} \left(2 + R^2 + \frac{2R^2 \Re z}{1 + |z|^2}\right) \exp\left(-\frac{1}{2}R^2 + \frac{R^2 \Re z}{1 + |z|^2}\right)$$

If $\xi \neq 0$, the pdf of Z is the pdf of $\exp(i\xi)\tilde{Z}$, where $\tilde{Z}$ has the pdf above. The Jacobian of the transformation obviously has determinant 1 ($\exp(i\xi)$ represents a rotation in $\mathbb{R}^2$ through ξ), so that the pdf is obtained by replacing z in the above formula by $z\exp(-i\xi)$. As the term $|z|^2$ remains unchanged, the result of the lemma follows.

References

[1] M.P. Paidoussis, "Dynamics of Flexible Slender Cylinders in Axial Flow; Part I, Theory; Part II, experiment", J. of Fluid Mechanics, vol. 26, pp. 717–751, 1966.

[2] R.M. Kennedy, "Crosstrack Dynamics of a Long Cable Towed in the Ocean", Oceans, pp. 966–970, 1981.

[3] R.M. Dowling, "The Dynamics of Towed Flexible Cylinders, Part I and II", J. of Fluid Mechanics, vol. 187, pp. 507–517, 1988.

[4] D.A. Gray, B.D.O. Anderson and R.R. Bitmead, "Models for the Application of Kalman Filtering to the Estimation of the Shape of a Towed Array", Proc. NATO Adv. Study Inst. on Underwater Acoustic Data Processing, Kingston, Ontario, Canada, 18–29 July, 1988.

[5] J. L. Riley, D.A. Gray and D.A. Holdsworth, "Estimating the Positions of an Array of Receivers Using Kalman Filtering Techniques", Proc. Int. Symp. on Sig. Proc. and Applications, Gold Coast, Australia, 27–31 August, 1990, pp. 364–367.

[6] B.G. Ferguson, "Sharpness Applied to the Adaptive Beamforming of Acoustic Data from a Towed Array of Unknown Shape", J. Acoustic Soc. America, vol. 88, p. 2695–2701, 1988.

[7] B.G. Ferguson, D.A. Gray and J.L. Riley, "Comparison of Sharpness and Eigenvector Methods for Towed Array Shape Estimation", J. Acoustic Soc. America, vol.91, pp. 1565–1570, 1992.

[8] R.L. Streit and R.F. Barrett, "Frequency Line Tracking Using Hidden Markov Models", IEEE Trans. ASSP, vol. 38, pp. 586–598, 1990.

[9] R.F. Barrett and D.A. Holdsworth, "Frequency Tracking Using Hidden Markov Models With Amplitude and Phase Information", (IEEE Transactions on Signal Processing - to be published).

List of Figures

1 Wavefront arriving at array, and sensor positions 3

2 Examples of the shapes generated by the HMM and sinusoidal array shape generation procedures. 10

3 Scatter plot of bearing (degrees) versus SNR (dB) scatter plot for $\mu = 4$ degrees and HMM shape. The dashed line indicates the true bearing. 11

4 Root mean square error (in degrees) versus SNR (dB) for $\mu = 4$ degrees and HMM shape. The solid line shows the HMM technqiue results and the dashed line shows the maximum likelihood technique results. 12

5 Scatter plot of bearing (degrees) versus SNR (dB) scatter plot for $\mu = 10$ degrees and HMM shape. The dashed line indicates the true bearing. 12

6 Root mean square error (in degrees) versus SNR (dB) for $\mu = 10$ degrees and HMM shape. The solid line shows the HMM technqiue results and the dashed line shows the maximum likelihood technique results. 13

7 Scatter plot of bearing (degrees) versus SNR (dB) scatter plot for $\mu = 4$ degrees and sinusoidal shape. The dashed line indicates the true bearing. 14

8 Root mean square error (in degrees) versus SNR for $\mu = 4$ degrees and sinusoidal shape. The solid line shows the HMM technqiue results and the dashed line shows the maximum likelihood technique results. 14

9 Scatter plot of bearing (degrees) versus SNR (dB) scatter plot for $\mu = 10$ degrees and sinusoidal shape. The dashed line indicates the true bearing. 15

10 Root mean square error (in degrees) versus SNR (dB) for $\mu = 10$ degrees and sinusoidal shape. The solid line shows the HMM technqiue results and the dashed line shows the maximum likelihood technique results. 15

11 Sensor position scatter plots for the HMM (top) and maximum likelihood methods (bottom) for SNR = -20dB. The true array shape is indicated by the solid line. 17

12 Sensor position scatter plots for the HMM (top) and maximum likelihood methods (bottom) for SNR = -30dB. The true array shape is indicated by the solid line. 17